Collisionless "thermalization" in the sheath of an argon discharge

David Coulette and Giovanni Manfredi

Citation: Physics of Plasmas (1994-present) **22**, 043505 (2015); doi: 10.1063/1.4917239
View online: http://dx.doi.org/10.1063/1.4917239
View Table of Contents: http://scitation.aip.org/content/aip/journal/pop/22/4?ver=pdfcov
Published by the AIP Publishing

Collisionless "thermalization" in the sheath of an argon discharge

David Coulette[a] and Giovanni Manfredi[b]
Institut de Physique et Chimie des Matériaux de Strasbourg, CNRS and Université de Strasbourg, BP 43, F-67034 Strasbourg, France

(Received 13 January 2015; accepted 30 March 2015; published online 9 April 2015)

We performed kinetic Vlasov simulations of the plasma-wall transition for a low-pressure argon discharge without external magnetic fields, using the same plasma parameters as in the experiments of Claire *et al*. [Phys. Plasmas **13**, 062103 (2006)]. Experimentally, it was found that the ion velocity distribution function is highly asymmetric in the presheath, but, surprisingly, becomes again close to Maxwellian inside the sheath. Here, we show that this "thermalization" can be explained by purely collisionless effects that are akin to the velocity bunching phenomenon observed in charged particles beams. Such collisionless thermalization is also observed in the presheath region close to the sheath entrance, although it is much weaker there and in practice probably swamped by collisional processes (standard or enhanced by instabilities). © *2015 AIP Publishing LLC*.
[http://dx.doi.org/10.1063/1.4917239]

I. INTRODUCTION

Plasma–surface interactions are a ubiquitous feature of virtually all types of laboratory plasma experiments. They occur whenever a plasma comes in contact with a material surface, such as a probe or a confining vessel. In magnetic confinement fusion experiments, plasma–surface interactions are of paramount importance for the understanding and control of the power load on a tokamak divertor plate, which constitutes one of the major challenges of current fusion research.

One of the most prominent features of the plasma–surface interaction is the appearance of various sorts of sheaths and presheaths. These are boundary layers that ensure a smooth transition between the unperturbed equilibrium plasma and the surface. In the simplest situation of all, a weakly collisional and unmagnetized plasma is in contact with a perfectly absorbing surface (referred hereafter simply as the "wall"), whose electric potential can be either fixed by the experimentalist (biased wall) or depend self-consistently on the net flux of charges on the wall (floating potential). The plasma-wall transition occurs in two steps (from plasma to wall): an extended quasi-neutral region with thickness of the order of the ion-neutral collision mean free path (presheath), followed by a thin nonneutral layer known as the Debye sheath (or simply the sheath). A well-known result (the Bohm Criterion) states that the ion velocity at the entrance of the Debye sheath must be equal to or larger than the sound speed.[1]

Under the combined action of the electric field and the ion-neutral collisions, the ion velocity distribution function (IVDF) in the plasma-wall transition region (presheath and sheath) can deviate significantly from a Maxwellian distribution, as was observed many times in experiments as well as numerical simulations.[2,3] In particular, the IVDF develops a broad and asymmetric low-velocity tail in the presheath, which can lead to an overestimation of the ion "temperature" if the latter is naively defined as the width of the IVDF.[4]

Unexpectedly, it was observed in recent experiments that the IVDF becomes again symmetric and almost Maxwellian (within the apparatus resolution) inside the sheath[5] or within the presheath.[6] This observed thermalization is surprising, because ion–ion collisions are negligible in the sheath, and also weak in the presheath region. In the present work, we address this problem by performing accurate numerical simulations based on a Vlasov code. Vlasov codes are particularly adapted to this kind of study, because they display a fine resolution in all regions of the phase space, including the sheath, where the plasma density is very low. We shall concentrate on the experimental results obtained by Claire *et al*.[5] using Laser Induced Fluorescence (LIF) measurements. As the sheath is very thin—just a few millimeters in a standard laboratory plasma discharge—measuring the IVDF inside the sheath is a daunting experimental challenge. Among plasma diagnostics, LIF is a privileged technique to obtain the IVDF with good spatial and velocity resolution without perturbing the plasma.[7–12]

The results of Claire *et al*.[5] show that the IVDF, after having developed a prominent asymmetric tail in the presheath, becomes again symmetric in the sheath. Here, we will show that this phenomenon can be explained using purely collisionless arguments, without invoking either ordinary or instability-enhanced[13,14] collision rates. Such symmetrization appears simply as a ballistic effect due to the different orbits of fast and slow particles in the phase space.

As to the presheath, the situation is more complicated. Recently, Yip *et al*.[6] reported that the IVDF thermalizes even within the presheath, in a region not far from the sheath entrance. Such behavior may be attributed to ion–ion collisions, but this interpretation is not self-evident, as ion–ion collisions are weak in the presheath for the plasma regime considered in the experiments. In order to explain the thermalization occurring in the presheath, the authors suggested that the plasma effective collisionality may be enhanced by

[a]Electronic mail: David.Coulette@ipcms.unistra.fr
[b]Electronic mail: Giovanni.Manfredi@ipcms.unistra.fr

the presence of instabilities (in particular, the ion-acoustic instability).[13,14] This instability-enhanced collisionality was used successfully to explain, for instance, the Bohm Criterion for multiple ion species plasmas.[10,11,15]

Our own results show that the collisionless thermalization that we observe in the sheath actually already begins in the presheath, although it is much more prominent in the former than in the latter. Indeed, we observed that around 10%–15% of the loss of asymmetry in the IVDF (as quantified precisely in Sec. III) already occurs in the presheath, the rest taking place in the sheath. Thus, although ion–ion collisions—in the form of the enhanced collisionality proposed by Baalrud *et al.*[13,14]—are probably responsible for most of the thermalization observed in the presheath,[6] we suggest that purely collisionless (ballistic) effects also play a minor, but perhaps not negligible, role.

The current paper is organized as follows: Section II will be devoted to the description of the main discharge parameters and the evaluation of the hypotheses underlying the kinetic model used in the simulations. In Sec. III, we will use the code to study the general properties of the plasma-wall transition in the regime of the experiments. Finally, we will examine in more detail the evolution of the distribution function in the sheath and its purported thermalization.

II. KINETIC MODELING OF THE ARGON DISCHARGE

A. Discharge parameters

The experimental setup used as reference for our simulations is described in Ref. 5. It consists of a cylindrical chamber of diameter 40 cm and length equal to 80 cm. The device is bounded by two conducting plates at the local floating potential. At roughly 8 cm from the cylindrical wall, the plasma is effectively unmagnetized.

The plasma is produced through ionization of the argon gas by a population of highly energetic (50–100 eV) electrons. These so-called primary electrons are generated by thermoemission and accelerated by means of a constant discharge potential. Two distinct populations of electrons thus coexist: the low-density, high-energy primary electrons, and the bulk electrons produced from ionization of the neutral atoms by impact with the primaries. The bulk electrons have lower energy and a much higher density (basically identical to the ion density, except in the sheath). The estimated characteristics of each particle population, taken from Ref. 5, are given in Table I.

The density ratio between primary and bulk electrons is low ($n_p/n_e \approx 10^{-3}$). As a consequence, the direct contribution of the primary electrons to space charge separation (coming from Poisson's equation) is negligible in the plasma.

TABLE I. Physical parameters of the argon discharge, from Ref. 5.

	Ar^+	Bulk (secondary) e^-	Primary e^-
M (kg)	6.64×10^{-26}	9.1×10^{-31}	9.1×10^{-31}
T (eV)	0.027	2.5	Unknown
E_{drift} (eV)	0	0	$50 - 100$
$n\,(\text{m}^{-3})$	$n_i = 5.5 \times 10^{15}$	$n_e = 5.5 \times 10^{15}$	$n_p = 2.0 \times 10^{12}$

However, their large drift energy ($E_{\text{drift}} \sim 20 - 40\,T_e \approx 50 - 100\,\text{eV}$) is sufficient to overcome the potential well in the sheath that would be created in a plasma containing only bulk electrons. Thus, the charge surface and the electric potential of the floating wall are mainly controlled by the primary electron current reaching the wall. This hypothesis is supported by the experimental measurement of the ion drift velocity profile near the wall.[5] In the case of a 50 V discharge (which will be considered in the remainder of this work), the ion maximum drift velocity in the sheath reaches values of about $6c_s$, implying a potential drop of the order of the discharge potential. In comparison, using a model including only bulk electrons with $T_e = 2.5\,\text{eV}$ would lead to a peak ion drift velocity of only $3c_s$. In summary, the primary electron density can be safely neglected in Poisson's equation. Instead, the primary electron current almost entirely determines the value of the electric potential on the floating wall. Therefore, in our simulations, the effect of the primaries will be modeled simply by biasing the wall at the discharge potential.

Finally, we note that, in contrast to the work of Claire *et al.*[5] the experiments of Yip *et al.*[6] (also considered later in this work) directly use a biased wall with $e\phi_{wall} = -50k_BT_e$. But from the point of view of our model, the situation is not that different: in both cases, the wall potential is roughly $e\phi_{wall} \approx 1800k_BT_i$, which implies a strong acceleration regime for the ions. Another difference is that Yip *et al.* work with a xenon plasma. Otherwise, the conditions of density, temperature, and pressure are similar to those of Ref. 5.

B. Physical model and numerical implementation

In the work of Claire *et al.*,[5] the IVDF is determined experimentally by LIF diagnostic near the central axis of the device. LIF measurements along the transverse dimensions on this axis show no significant departure from thermal equilibrium. The system can thus be considered as invariant along those dimensions, leading to a one-dimensional model in the x coordinate along the central axis. As the plasma is unmagnetized in this region, the description of the velocity space can also be reduced to only one velocity coordinate v_x along the axis.

The argon ion population is thus described by a 1D-1 V kinetic model through the evolution of the distribution function $f_i(x, v_x, t)$. The bulk electrons could also be described by a kinetic model, but this would lead to a significantly larger numerical complexity. Alternatively, since the electron-to-ion mass ratio is very small, the electron population can be considered at thermal equilibrium and its evolution described by means of the Boltzmann law: $n_e = n_{e0}\exp[e(\phi - \phi_{ref})/k_BT_e]$. For most results presented hereafter, the Boltzmann model will be used for the electrons. Comparisons with fully kinetic simulation (see Sec. II C) showed no significant impact of the Boltzmann approximation on the ion velocity distribution in the stationary state.

Primary electrons are difficult to model as their exact distribution is unknown, and their introduction would require, for consistency, the inclusion of further species

(neutrals) and collisional processes to the model, which is out of the scope of the present work. As mentioned before, the primary electrons' direct contribution to space charge density is negligible compared to bulk electrons, but the primary electrons' current has a major impact on the wall potential. To mimic this effect, we neglect altogether the primary electron density in the Poisson equation, and replace the floating potential at the wall with a fixed potential of the order of the discharge one ($\phi_{wall} = 50\,\mathrm{V}$ in the rest of this work). In this way, we ensure that the depth of the potential well in the sheath is similar to the one observed experimentally, leading to a comparable velocity range for the ion longitudinal drift velocity.

Collisional processes are modeled by a single Bhatnagar–Gross–Krook (BGK)[16] linear relaxation operator $\mathcal{C}_s$ driving the distribution function toward a Maxwellian: $\mathcal{C}_s = -\nu_{bgk}(f - f_M)$, where ν_{bgk} is the relaxation rate and f_M is a spatially homogeneous Maxwellian with bulk plasma parameters. For the ions, the BGK operator models primarily ion-neutral charge exchange collisions, which dominate over ion–ion Coulomb collisions in the regime of interest here. With these assumptions, the evolution of the distribution function of species s is described by the Vlasov equation

$$\partial_t f_s + v_x \partial_x f_s + \frac{q_s}{m_s} E_x \partial_{v_x} f_s + \nu_{bgk}(f_s - f_M) = 0, \qquad (1)$$

and the electric field $E_x = -\partial_x \phi$ is obtained by solving Poisson's equation for the electrostatic potential,

$$\Delta\phi + \frac{1}{\epsilon_0}\sum_s q_s \int_{-\infty}^{\infty} f_s dv_x = 0. \qquad (2)$$

When a Boltzmann law is used for the electron response, Eq. (2) becomes nonlinear and is solved iteratively. With such a simple model for plasma processes, we cannot expect a precise quantitative agreement with experimental data, particularly at the entrance of the sheath where the IVDF evolves rapidly, both in position and shape. In spite of these limitations, Eqs. (1) and (2) were used in the past to model this type of physics and showed very reasonable agreement with experimental measurements.[2]

The numerical simulations were performed using an Eulerian finite-volume kinetic code.[17,18] Realistic discharge parameters impose the use of fine grids both in real and velocity space if one wants to properly describe the full evolution of the distribution functions from the bulk plasma to the wall. Since the spatial gradients are expected to be much smaller in the presheath than in the sheath, the spatial dimension x is sampled using a non-uniform grid, and we only simulate one half of the plasma, between the bulk (on the right-hand side) and the wall (located at $x = 0$ on the left, see Fig. 1). The cell width ranges from a fraction of the Debye length (here, $\lambda_D = 1.59 \times 10^{-4}\mathrm{m}$) in the sheath to hundreds of λ_D in the presheath. The domain size is set to sufficiently large values compared to the ion mean free path to ensure a smooth transition between the presheath and the bulk plasma at the right boundary, where a Maxwellian plasma is assumed.

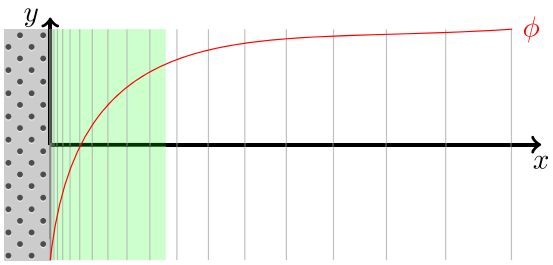

FIG. 1. Geometry of the model. The vertical lines represent the grid points. The sheath (leftmost region, in green) is finely resolved ($\Delta x \sim 0.05\lambda_D$), whereas the grid spacing gets coarser in the presheath (on the right). At the boundary with the bulk plasma ($x \approx 10^5 \lambda_D$), the grid spacing is $\Delta x \sim 500\lambda_D$.

The simulations are initialized with a spatially uniform Maxwellian plasma $f_s(t = 0) = f_M$, which is then let to evolve according to Eqs. (1) and (2) until the steady-state solution is attained. This typically occurs after several ion collision times $\tau = \nu_{bgk}^{-1} \sim 10^3 - 10^5\, \omega_{pi}^{-1}$.

C. Validity of the Boltzmann approximation for the electrons

In order to assess the impact of the use of a Boltzmann response for the electrons, a few simulations were run with a kinetic treatment for both ions and electrons. The fully kinetic simulations were performed with two different kinds of initial conditions. In the first case, the distributions of both species are set initially to uniform Maxwellian distributions with bulk plasma parameters. In the second case, the initial state is equal to the steady state obtained with the Boltzmann model for the electrons. We then verified that the steady-state distributions obtained with either initial conditions were identical, although, of course, the transients were different. As a consequence, we will not make any further distinction between the two kinds of initial conditions and indiscriminately refer to the corresponding simulations as the "kinetic electron" simulations.

We first compare the steady-state electronic density (Fig. 2(a)) and the electrostatic potential (Fig. 2(b)) obtained from simulations using the kinetic and the Boltzmann models for electrons. We observe an overall very good agreement for both profiles on the entire spatial domain. Some small discrepancies appear in the vicinity of the wall, well inside the sheath ($x < 5\lambda_D$), where the values of the electron density are extremely low anyway ($n_e \approx 10^{-3} - 10^{-4} n_{e0}$).

The electron velocity distribution function remains close to a Maxwellian up to the sheath entrance (Fig. 3(a)), but it is strongly perturbed near the wall (Fig. 3(b)). Although the two models yield significantly different results in the sheath for the distribution functions, the impact on the potential profile (Fig. 2(b))—and consequently on the ion distribution—remains negligible since the space charge density in that region is dominated by the ions. Indeed, the ion density and average velocity profiles obtained with either electron models (Boltzmann and kinetic) display excellent agreement, as shown in Fig. 4.

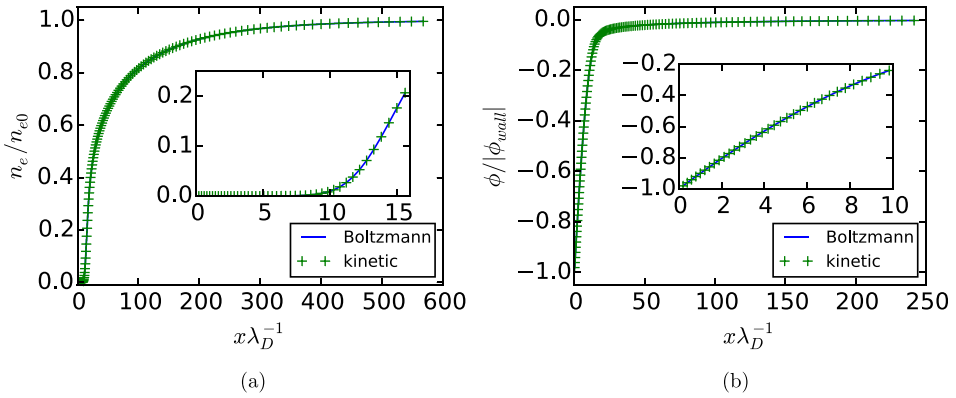

FIG. 2. Comparison of the steady-state profiles obtained with kinetic and Boltzmann electrons: the electron density (a) and the electrostatic potential (b).

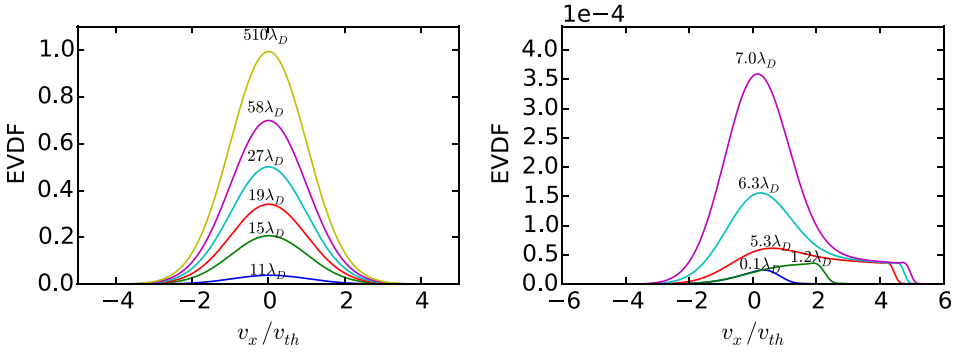

FIG. 3. Electron velocity distribution function, normalized to its peak value in the bulk plasma, at several positions in the presheath (a) and in the sheath (b).

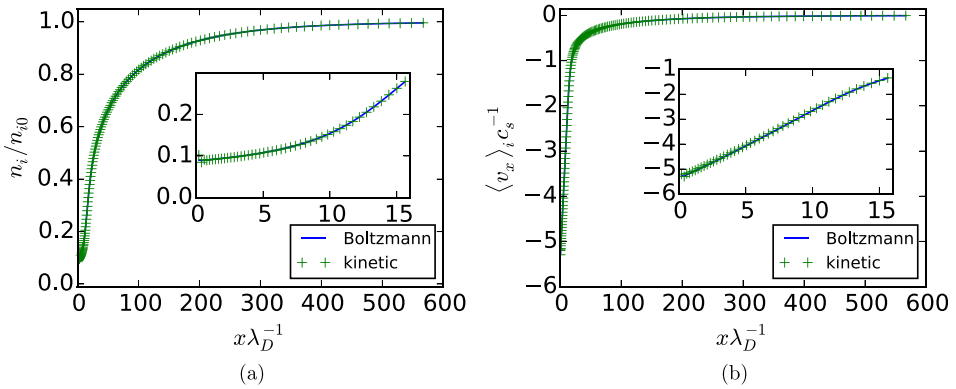

FIG. 4. Comparison of the steady-state profiles obtained with kinetic and Boltzmann electrons: the ion density (a) and the ion mean velocity (b).

III. NUMERICAL RESULTS ON THE PLASMA-WALL TRANSITION

A. Effect of the relaxation frequency

As all collisional processes in our model are contained in a single BGK operator, its frequency ν_{bgk} cannot be fixed precisely from experimental parameters. Observation of the experimental IVDF profiles and simple estimations of the collision rates of the dominant plasma processes can only provide the order of magnitude of ν_{bgk}. Using an estimation of the reaction rates[19–23] for ionization and charge exchange of about $R \sim 10^{-15} - 10^{-14}\mathrm{m}^3\mathrm{s}^{-1}$, and a discharge pressure $P = 4.8 \times 10^{-4}\,\mathrm{mbar} = 0.36\,\mathrm{mTorr}$, the corresponding relaxation frequencies range from $7 \times 10^{-4}\omega_{pi}$ to $10^{-3}\omega_{pi}$. Therefore, we have performed a parametric scan in the frequency of the BGK operator, with values ranging from $\nu_{bgk} = 10^{-4}\omega_{pi}$ to $\nu_{bgk} = 7.5 \times 10^{-2}\omega_{pi}$.

In addition to the fixed frequency BGK relaxation [Eq. (1)], two further models were considered, for which the reference relaxation frequency ν_{bgk} is multiplied by a factor that takes into account the local ion velocity distribution function. The first model is dubbed "constant mean-free-path" and the corresponding definition of the frequency is as follows:

$$\nu_{cmfp} = \nu_{bgk} \sqrt{\frac{\langle (v_x - \langle v_x \rangle)^2 \rangle_i}{T_0}}. \tag{3}$$

In this model, the frequency grows in the presheath as the ion distribution widens, but decays again in the sheath. The second model, which we refer to as the "friction" model, is based on the second-order velocity moment of the IVDF

$$\nu_{fric} = \nu_{bgk} \sqrt{\frac{\langle v_x^2 \rangle_i}{T_0}}. \tag{4}$$

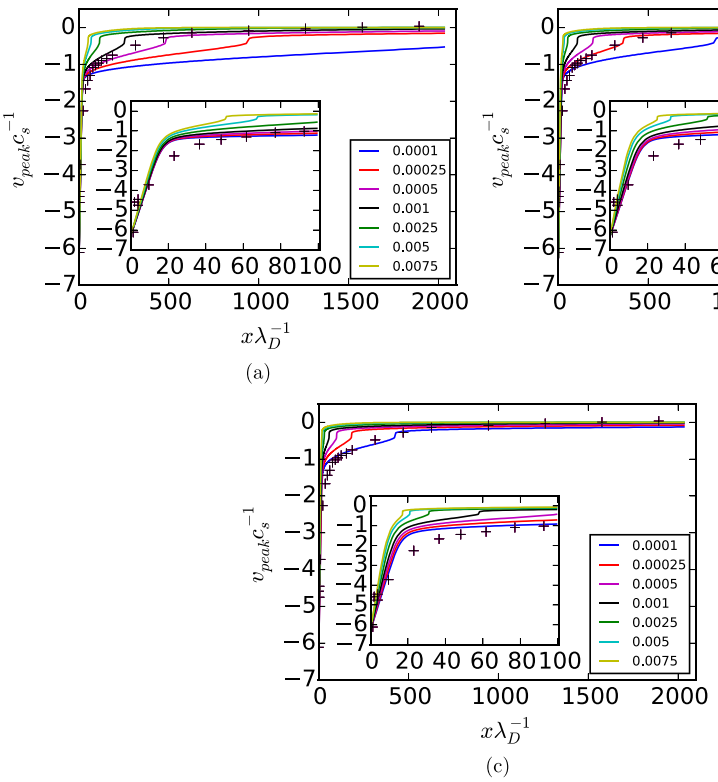

FIG. 5. Spatial profiles of the ion peak velocity v_{peak} for different values of the BGK frequency and different relaxation models: constant relaxation rate operator (a); constant mean-free path operator (b); and friction operator (c). LIF data taken from Fig. 10 of Ref. 5 for a discharge pressure of 4.8×10^{-4}mbar are indicated by crosses. The BGK relaxation rates ν_{bgk}, in units of ω_{pi}, are shown in the insets.

In this second model, the relaxation frequency can grow both from the widening and from the global acceleration of the ion distribution function.

In order to compare our simulation results with the measurements obtained in Ref. 5, we consider the evolution of the velocity v_{peak} corresponding to the peak of the IVDF as a function of the distance from the wall x. Results of the parametric scans in the relaxation frequency ν_{bgk} are shown in Fig. 5. Let us first consider the profiles at a distance $x > 60\lambda_D$ from the wall. For each relaxation operator type, some value of the reference relaxation frequency appears to provide a partial match of the simulation results with the experimental data. In the constant rate case (Fig. 5(a)), the best-match frequency is between $5 \times 10^{-4}\omega_{pi}$ and $10^{-3}\omega_{pi}$, which is consistent with our estimation. For the two other operators, the closest match is obtained for $\nu_{bgk} = 2.5 \times 10^{-4}\omega_{pi}$, (Fig. 5(b)) and $\nu_{bgk} = 10^{-4}\omega_{pi}$ (Fig. 5(c)). Overall, in this region, the agreement between simulations and experimental results is quite good.

For positions between $x = 10\lambda_D$ and $x = 60\lambda_D$, corresponding to the entrance of the sheath, we observe a slight but systematic departure of the simulation data from the experimental measurements, for which the transition at the entrance of the sheath is smoother. Extrapolating the dependency of the simulation profiles with ν_{bgk}, it does not seem possible to fit the experimental data on the entire spatial domain. In the context of our model, no clear explanation can be given for the observed discrepancy in this region. In Ref. 5, the authors mentioned a noticeable increase in the LIF signal intensity in this particular region. This phenomenon was observed elsewhere,[24] but never fully explained. In the context of the present analysis, we take it as an indication that some physical processes unaccounted for by our model must occur in that region. Nevertheless, considering the many approximations that are inherent to the model, the agreement obtained with the experimental data is still rather satisfactory.

Finally, for completeness, we show in Fig. 6 the profiles of the relative charge density (Fig. 6(a)) and the corresponding ion average velocity (Fig. 6(b)). Taking for instance $|\rho/q_i n_i| \approx 2\%$ as a significant departure from quasi-neutrality, the sheath-presheath boundary is situated around

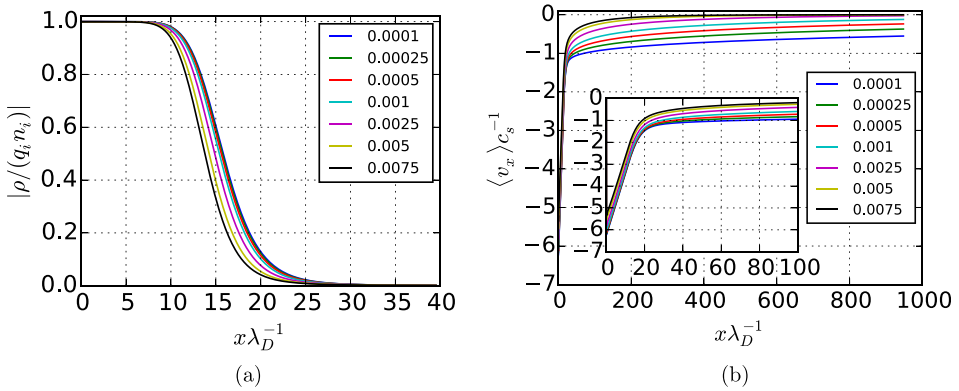

FIG. 6. Spatial profiles of the charge density normalized to the local ion density (a) and the average ion velocity (b), for different values of the BGK frequency (constant relaxation rate operator). The BGK rates ν_{bgk}, in units of ω_{pi}, are shown on the figure.

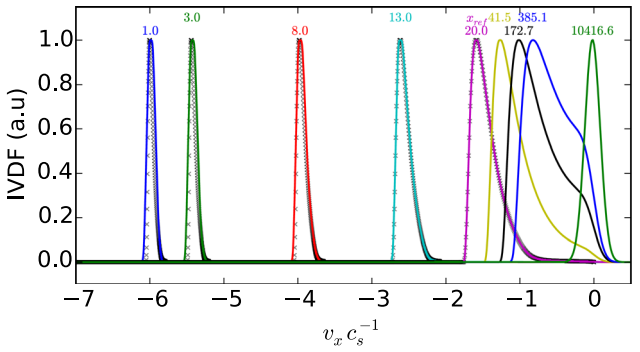

FIG. 7. Global evolution of IVDF profiles from bulk to wall for a case with $\phi_{wall} = 50$ V and $\nu_{bgk} = 2.5 \times 10^{-4}$ (constant frequency model). The distribution functions are normalized to their peak value at each location. The distance from wall, expressed in units of λ_D, is shown above each peak. The crosses are the results of the ballistic model described in the main text, with $x_{\mathrm{ref}} = 20\lambda_D$.

$20 - 25\lambda_D$ from the wall for all values of the collision frequency considered here. As can be seen on Fig. 6(b), this definition of the sheath entrance is consistent with the standard Bohm Criterion for weakly collisional plasmas, i.e., the requirement that $u_i \geq c_s$ at the entrance of the sheath, with no appreciable collision-induced corrections.[25,26]

B. Evolution of the IVDF from bulk to wall

The overall evolution of the IVDF from the bulk plasma to the wall is very similar to the experimental results. An example of such an evolution is given in Fig. 7. Starting from a Maxwellian shape in the bulk plasma, the distribution becomes noticeably asymmetric in the presheath (for instance at $x = 385\lambda_D$). This structure is similar to that predicted by the Emmert model.[27] Near the sheath entrance ($x \approx 20\lambda_D$), the "shoulder" of the distribution gets flattened out, and inside the sheath, the distribution becomes again symmetric.

We shall discuss further on whether this effect can be considered a sign of the "Maxwellianization" or thermalization of the IVDF. For the time being, we point out two facts. First, the asymmetric tail in the IVDF is due to a competition in the presheath between the electric field (which tends to accelerate the ions toward the wall) and the BGK relaxation term (which drives the IVDF toward a zero-mean Maxwellian). Second, the evolution in the sheath is almost collisionless—as the sheath is much thinner than the collisional mean free path—and therefore dominated by the electric field.

The first fact can be assessed by looking at the IDVF at the entrance of the sheath. For larger values of the relaxation frequency ν_{bgk}, the asymmetric tail is more prominent, as can be seen from Fig. 8. This is in line with the experimental measurements of Refs. 5 and 6, where it was pointed out that the asymmetry of the IVDF comes essentially from the ion-neutral collisions. In Fig. 8(a), following Claire *et al.*,[5] we define the sheath entrance as the point where the ion velocity reaches the value $1.4c_s$. In Fig. 8(b), the sheath entrance is taken as the position where the charge separation becomes equal to 2% of the bulk density. With the first definition, the peaks of the IVDFs are not located at the same positions, whereas with the second definition, the peaks do not correspond to the same velocity.

The second fact can be checked by making use of a ballistic model for the sheath. We start from a given position x_{ref} with potential ϕ_{ref} and consider only negative velocities (i.e., directed toward the wall). In the absence of any collision, the distribution function is conserved along the characteristics $d(v^2 + \frac{2q_i}{m_i}\phi) = 0$, and can thus be written as

$$f(x,v) = f\left(x_{\mathrm{ref}}, v_{\mathrm{ref}} = -\sqrt{v^2 + \frac{2q_i}{m_i}(\phi(x) - \phi_{\mathrm{ref}})}\right). \quad (5)$$

The results of the ballistic model (using $x_{ref} = 20\lambda_D$, i.e., at the beginning of the sheath) are represented as crosses on Fig. 7 and match very well the profiles of the full simulations inside the sheath. Since the ions are strongly accelerated in the sheath, it is quite challenging from a computational point of view to reproduce the correct IVDF without too much numerical smearing. Thus, the results of Fig. 7 serve as a validation of the accuracy of our numerical method.

If the reference position is taken inside the presheath ($x_{ref} = 117\lambda_D$, see Fig. 9), the ballistic model still works pretty well, except for ions with small velocities in absolute value. These ions experience too many collisions as they advance toward the wall, so that the ballistic approximation breaks down for them: this explains the cut-off observed on the profiles at low velocities. All in all, Fig. 9 shows that, although we are definitely in the presheath (at $x_{ref} = 117\lambda_D$ the space charge density is virtually zero), ballistic effects still do play a role for a non-negligible part of the IVDF. Of course, when moving further into the presheath the cut-off on the IVDFs will shift to higher (more negative) velocities, until the entire ion distribution is affected by the collisions.

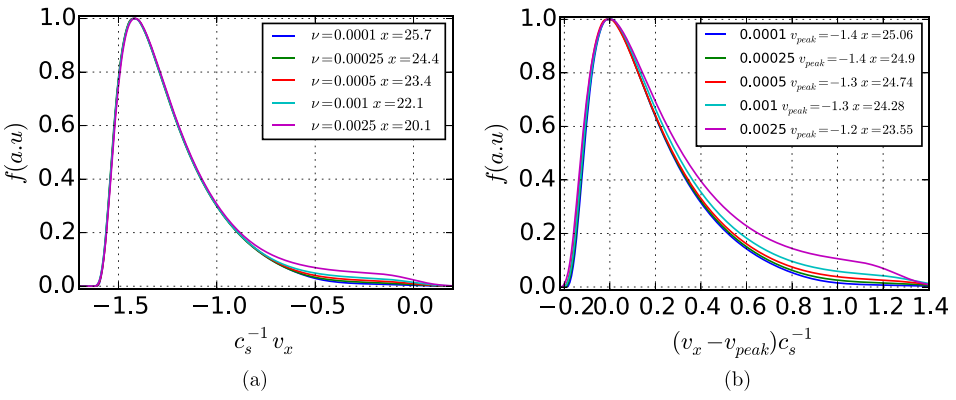

FIG. 8. IVDFs at the entrance of the sheath for different values of the BGK relaxation frequency. The sheath entrance is defined as the point where the peak velocity reaches $1.4c_s$ (a) or as the point where the charge separation becomes equal to 2% of the bulk density (b). The insets indicate the spatial location of the IVDFs in units of λ_D (a) as well as the velocity of the peaks in units of c_s (b). For clarity, in (b), all the IVDFs have been centered on the position of their peak.

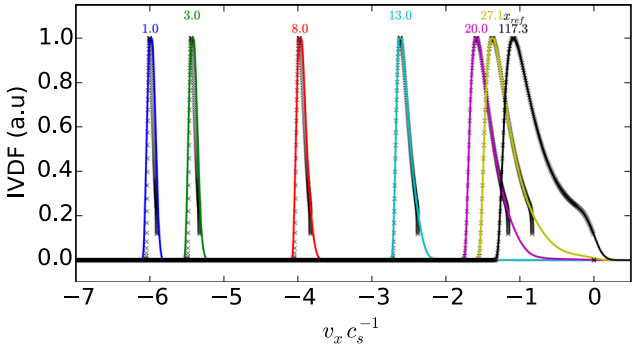

FIG. 9. Evolution of IVDF profiles from the reference position $x_{\text{ref}} = 117.3\lambda_D$ to the wall for a case with $\phi_{wall} = 50\text{V}$ and $\nu_{bgk} = 2.5 \times 10^{-4}$ (constant frequency model). The distribution functions are normalized to their peak value at each location. The crosses are the results of the ballistic model described in the main text.

We will come back to this in Sec. III C, when discussing the presheath thermalization observed by Yip *et al.*[6]

This is also an important issue for the experimental results of Ref. 5, where the potential profile was not measured directly, but rather inferred from the conservation of energy, which is only valid in the absence of collisions. Indeed, the potential drop across the presheath is a sharply increasing function of the neutral pressure, as was shown in Ref. 28. Our results are a clear indication that we are working in the low-collisionality regime, so that the method of Claire *et al.* to arrive at the potential profiles is indeed justified not only in the sheath but also in the presheath region close to the sheath entrance.

C. Symmetry properties

We now examine more precisely the evolution of the symmetry properties of the IVDF. In the presheath, the ion velocity distribution is highly skewed. This asymmetry, as we have seen, is due to the competition between the electric field and the BGK term (ion-neutral exchange collisions). However, as the ions accelerate in the sheath, the IVDF tends to appear more and more symmetric as its tail is flattened, as can be seen from Fig. 10. This effect is purely ballistic and stems from the contracting nature of the velocity transformation along the characteristics described by Eq. (3). Setting $\Delta v^2 \equiv v^2 - v_{\text{ref}}^2 = -2\frac{q_i}{m_i}(\phi - \phi_{\text{ref}}) > 0$, the Jacobian of the velocity transformation along a constant energy characteristic reads as

$$\mathcal{J} = \left|\frac{dv}{dv_{\text{ref}}}\right| = \left|\frac{v_{\text{ref}}}{v}\right| = \frac{|v_{\text{ref}}|}{\sqrt{v_{\text{ref}}^2 + \Delta v^2}}. \tag{6}$$

This mapping is always contracting ($\mathcal{J} \leq 1$) and more so for the trajectories with lower initial velocities ($\mathcal{J}$ is an increasing function of $|v_{ref}|$). Simply put, this means that slow ions get more strongly accelerated than fast ions, so that the low-velocity tail "catches up" with the main lobe of the distribution, making the IVDF look more symmetric. This is clearly seen in Fig. 10(a), where the dashed lines represent each distribution function symmetrized with respect to the position of its own peak. As one approaches the wall, the distributions become obviously narrower and more symmetric. This is akin to the so-called velocity-bunching effect in accelerated beams of charged particles.[29]

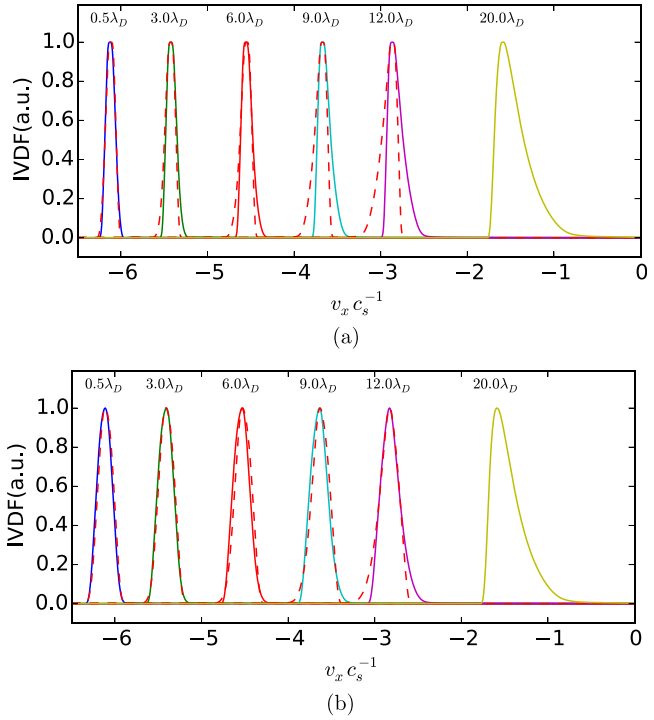

FIG. 10. IVDF in the sheath for raw simulation data (a) and for simulation data convolved with a moving average filter of width $\Delta x = 0.125\,\text{mm} \approx 0.79\lambda_D$ (b). The BGK relaxation rate is $\nu_{bgk} = 2.5 \times 10^{-4}\omega_{pi}$. The dashed lines represent the mirror image of each distribution with respect to its peak.

Strictly speaking, the asymmetric tail never disappears—it is just stretched by the ballistic velocity transformation and remains at very low level. Therefore, this asymmetry can easily be masked by the uncertainty arising from the finite resolution and background noise level of the experimental apparatus (in the case of experiments) or from numerical diffusion and/or noise (in the case of computer simulations, particularly those using particle-in-cell codes). In the case of LIF diagnostics, the actual signal results from a volume integral whose size depends on the diaphragm slit aperture and optical system used to collect the signal. For the 50 V discharge of Claire *et al.*[5] discussed here, the slit width is $\Delta x = 0.125\,\text{mm} \approx 0.79\lambda_D$.[30] Although this is sufficiently small (relative to the electric field gradient) to make the spatial averaging effect negligible for most quantities of interest, it may still have a significant impact on the skewness of the IVDF. In order to assess the effect of a finite slit width in our simulations, we have convolved the raw distribution functions with a gate function of width $\Delta x = 0.79\lambda_D$.[4] A comparison of the raw and filtered distribution functions at several positions in the sheath is shown in Fig. 10. The effect of the averaging filter on the position and typical width of the distribution is rather modest. Nevertheless, the symmetry properties of the distributions are affected at distances $x < 12\lambda_D$, for which the skewness of the main lobe of the distribution is significantly reduced.

The above convolution effect may also explain the results for the 100 V discharge of Claire *et al.* (Fig. 8 in Ref. 5), for

which the IVDF actually widens further and further into the sheath. Indeed, a large electric field means that the IVDF evolves quickly along different spatial locations in the sheath. If this fast variations cannot be resolved, the experimental apparatus will average (convolve) the IVDF over different spatial locations and the measured IVDF will look wider than it is in reality. This type of "convolution heating" (which can lead to an overestimation of the ion temperature) was observed in Ref. 3 and interpreted in Ref. 4.

To quantify more precisely the symmetrization of the IVDF, we have considered several functionals measuring the asymmetry of the distribution. The standard skewness can actually be misleading because it gives a disproportionate weight to the tail of the distribution, which is generally very low-level and thus lost in the (numerical or experimental) noise. Instead, what we would like to measure is the asymmetry of the main lobe of the distribution.

For this purpose, we shall use two functionals. The first functional can be viewed as a zeroth-order skewness relative to the distribution peak, and is defined as follows:

$$\gamma^{(0)} = \frac{\int_{-\infty}^{v_{\text{peak}}} f dv - \int_{v_{\text{peak}}}^{+\infty} f dv}{n}, \tag{7}$$

where $n = \int_{-\infty}^{\infty} f dv$. Basically, this functional computes the difference between particles having velocities smaller than v_{peak} and particles having velocities larger than v_{peak}, which is zero for a symmetric distribution. The second functional is the Maxwellian fit used by Yip *et al.*[6]

$$R_{\text{fit}} = \frac{\int_{-\infty}^{\infty} [f(v) - f_{\text{fit}}(v)] dv}{n}, \tag{8}$$

where $f(v)$ is the IDVF issued from the simulations and $f_{\text{fit}}(v)$ is a best-fit Maxwellian function with same peak velocity as $f(v)$; the fitting parameter is the variance of the Maxwellian function.

A comparison of the two functionals in the region of the sheath and beginning of the presheath is shown on Fig. 11, both for the raw distributions and for the distributions filtered using the convolution procedure described earlier in this section. Both methods show clearly that the IVDF becomes almost perfectly symmetric within the sheath, with each skewness measure falling from 0.5 at the entrance of the sheath ($x \approx 20\lambda_D$) to 0.1 or less at the wall.

Several remarks are in order here. First, this apparent symmetrization of the IVDF is a purely collisionless effect, as it happens mainly in the sheath. It is interesting to note that the distribution can get closer to a Maxwellian (in a quantitative way measured by R_{fit}) even in the absence of collisions. This fact prompts us to state the main messages of the present work: The observed Maxwellianization (thermalization) of the IVDF in the sheath can be fully explained in terms of collisionless effects, without invoking collision rates, either ordinary or instability-enhanced.

Second, we note that for both functionals, the filtered curve is always lower than the raw curve, thus revealing the symmetrization effect of the convolution procedure, even for the very fine apparatus resolution used here ($\Delta x = 0.125\,\text{mm} \approx 0.79\lambda_D$). This leads us to our second message, namely, that even a very small level of experimental or numerical noise (not detected in other global quantities such as the average ion velocity) can have a significant impact on the symmetry properties of the IVDF.

If we look at larger distances from the wall (Fig. 12), we notice that both functionals $\gamma^{(0)}$ and R_{fit} attain a maximum around $x = 150\lambda_D$ (i.e., $\approx 130\lambda_D$ from the sheath entrance). Thus, the symmetrization of the IVDF begins inside the presheath, although the fall of R_{fit} and $\gamma^{(0)}$ is small in the presheath (about 10%–15% of the total fall) compared to that occurring in the sheath. Nevertheless, it is clear that the IDVF becomes more symmetric in the presheath even in the absence of ion–ion collisions. The fact that the symmetrization starts in the presheath stems from the universal nature of the so-called acceleration bunching of charged beams.[29] The effect is much larger in the sheath simply because the ion acceleration is stronger. But, a milder acceleration is also present in the presheath (see Fig. 4), which explains that some degree of symmetrization is observed there too.

Using the parameters of Ref. 6, where $\lambda_D \approx 0.16\,\text{mm}$, we deduce that the IVDF starts to symmetrize at about 20 mm ($\approx 130\lambda_D$) from the sheath entrance. This is roughly the same region where the collisionally induced thermalization is observed in that work. This prompts us to state our third and final message: Although the thermalization observed in the presheath[6] is well explained by enhanced-collisionality models, collisionless effects may also play a role, albeit probably a minor one.

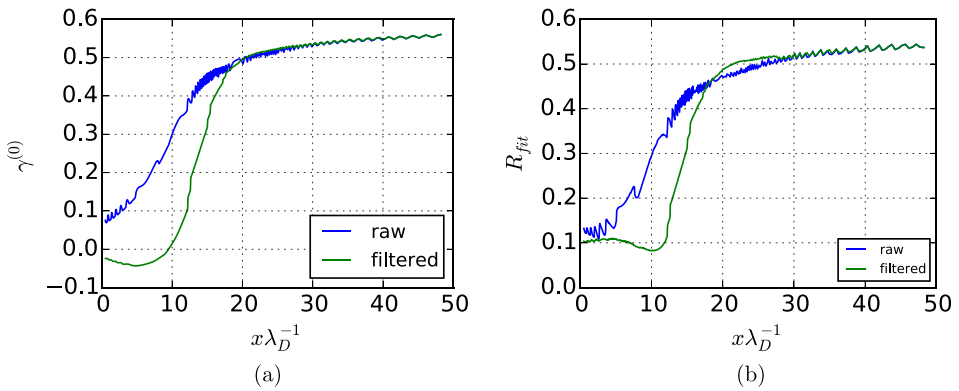

FIG. 11. Plots of the zeroth-order skewness $\gamma^{(0)}$ (a) and the Maxwellian fit function R_{fit} (b) as a function of the distance from the wall, computed using the raw distributions (blue curves) or the convolved distributions (green curves). The BGK relaxation rate is $\nu_{bgk} = 2.5 \times 10^{-4}\omega_{pi}$.

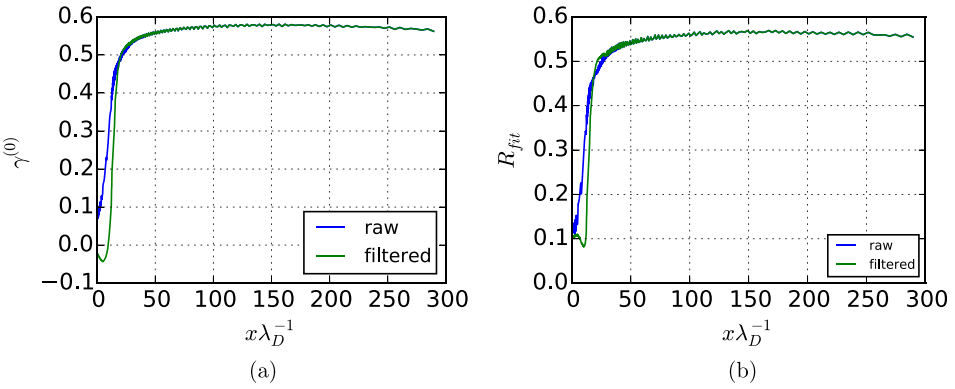

FIG. 12. Same as Fig. 11, for larger distances from the wall.

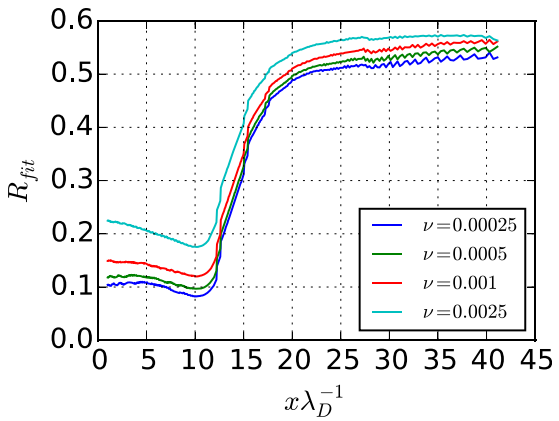

FIG. 13. Maxwellian fit function R_{fit} (from the filtered data) for different values of the BGK relaxation rate, expressed in units of ω_{pi}.

Finally, in Fig. 13, we show the behavior of the Maxwellian fit function R_{fit} for various values of the BGK relaxation rate. The drop is larger when ν_{bgk} is smaller, confirming again that the observed "thermalization" is a collisionless phenomenon.

IV. CONCLUSIONS

In a unmagnetized plasma-wall transition, the IVDF observed in the presheath is generally non-Maxwellian and indeed prominently asymmetric, an effect that is attributed to ion-neutral charge exchange collisions. However, recent experimental work has shown that the IVDF becomes again close to Maxwellian inside the sheath[5] or within the presheath.[6] This thermalization is at odds with the fact that ion–ion collisions are negligible in the sheath and generally weak in the presheath. To explain this surprising state of affairs, it was suggested that the plasma effective collisionality may be enhanced by the presence of instabilities.[13] Very recent experimental results seem to confirm this conjecture.[6]

In the present work, we have shown that collisionless effects may also play an important role in the thermalization. Our results can be summarized as follows:

- In the sheath, the "thermalization" can be achieved simply on the basis of ballistic (collisionless) effects that are akin to the velocity bunching observed in charged particles beams;
- The finite resolution of the experimental apparatus contributes to the thermalization of the IVDF, even when it does not affect other global quantities such as the ion mean velocity.
- Such collisionless thermalization already begins in the presheath, some $130\lambda_D$ from the sheath entrance for the case studied here—however, collisionless effects are probably insufficient to fully explain the Maxwellianization occurring in the presheath, and some collisional processes have to be invoked, as was done in Ref. 6.

We stress that our analysis was based on actual experimental parameters and a close comparison between the experimental data and the simulation results.

In summary, while the enhanced collisionality proposed by Baalrud *et al.*[13] certainly plays an important role on the thermalization observed in the presheath, one should not disregard the collisionless scenarios put forward in the present work.

ACKNOWLEDGMENTS

We thank Nicolas Claire for several useful discussions on the experimental setup and for providing some of the experimental data. The authors acknowledge the support of the French Agence Nationale de la Recherche (ANR) under reference No. ANR-12-BS09-028-01.

[1]D. Bohm, *Characteristics of Electrical Discharges in Magnetic Fields* (McGraw-Hill, New York, 1949), Vol. 1.
[2]S. Devaux and G. Manfredi, Phys. Plasmas **13**, 083504 (2006).
[3]G. Bachet, L. Chérigier, and F. Doveil, Phys. Plasmas **2**, 1782 (1995).
[4]G. Manfredi and F. Valsaque, Comput. Phys. Commun. **164**, 262 (2004).
[5]N. Claire, G. Bachet, U. Stroth, and F. Doveil, Phys. Plasmas **13**, 062103 (2006).
[6]C. Yip, N. Hershkowitz, and G. Severn, Plasma Sources Sci. Technol. **24**, 015018 (2015).
[7]G. D. Severn, D. A. Edrich, and R. McWilliams, Rev. Sci. Instrum. **69**, 10 (1998).
[8]A. M. Keesee, E. E. Scime, and R. F. Boivin, Rev. Sci. Instrum. **75**, 4091 (2004).
[9]L. Oksuz, M. A. Khedr, and N. Herschkowtiz, Phys. Plasmas **8**, 1729 (2001).
[10]G. Severn, X. Wang, E. Ko, and N. Hershkowitz, Phys. Rev. Lett. **90**, 145001 (2003).
[11]G. Severn, X. Wang, E. Ko, N. Hershkowitz, M. Turner, and R. McWilliam, Thin Solid Films **506–507**, 674 (2006).
[12]T. Lunt, W. B. G. Fussmann, and O. Waldmann, in 36th EPS Conference on Plasma Physics (2009).
[13]S. Baalrud, J. Callen, and C. Hegna, Phys. Rev. Lett. **102**, 245005 (2009).
[14]S. D. Baalrud and C. C. Hegna, Plasma Sources Sci. Technol. **20**, 025013 (2011).

[15]S. D. Baalrud, C. C. Hegna, and J. D. Callen, Phys. Rev. Lett. **103**, 205002 (2009).
[16]P. L. Bhatnagar, E. P. Gross, and M. Krook, Phys. Rev. **94**, 511 (1954).
[17]F. Filbet, E. Sonnendrucker, and P. Bertrand, J. Comput. Phys. **172**, 166 (2001).
[18]D. Coulette and G. Manfredi, J. Phys.: Conf. Ser. **561**, 012005 (2014).
[19]W. Lotz, Z. Phys. **232**, 101 (1970).
[20]S. Pullins, R. Dressler, R. Torrents, and D. Guerlich, Z. Phys. Chem. **214**, 1279 (2000).
[21]J. A. Hornbeck, J. Phys. Chem. **56**, 829 (1952).
[22]M. Lierbemann and A. Lichtenberg, *Principles of Plasma Discharges and Materials Processing* (John Wiley and Sons, Inc., 1994).
[23]D. Hodgkinson and J. Briggs, J. Phys. B: At., Mol. Opt. Phys. **9**, 255 (1976).
[24]M. Carrere, L. Cherigier, C. Arnas-Capeau, G. Bachet, and F. Doveil, Rev. Sci. Instrum. **67**, 4124 (1996).
[25]R. P. Brinkmann, J. Phys. D: Appl. Phys. **44**, 042002 (2011).
[26]H.-B. Valentini and D. Kaiser, Plasma Sources Sci. Technol. **23**, 015004 (2014).
[27]G. Emmert, R. Wieland, A. Mense, and J. Davidson, Phys. Fluids **23**, 803 (1980).
[28]A. Meige, O. Sutherland, H. B. Smith, and R. W. Boswell, Phys. Plasmas **14**, 032104 (2007).
[29]K. R. Anton, S. L. Kaufman, W. Klempt, G. Moruzzi, R. Neugart, E. W. Otten, and B. Schinzler, Phys. Rev. Lett. **40**, 642 (1978).
[30]Strictly speaking, one should use the image width of the slit projected backwards to the location of the laser beam, which depends on the effective magnification of optical system. However, this information is not provided by the authors of Ref. 5, which use the slit width as the relevant parameter. As a first approximation, we have thus supposed that the magnification is equal to unity.